

Supporting Information

Scholz et al. 10.1073/pnas.1615259114

SI NY Times Article Sample

We selected 80 articles from the full set of 760 articles analyzed in ref. 11 with the goal of maximizing comparability in topic and length. Specifically, we conducted a keyword search of the full set of 760 articles using the following terms: exercise, fitness, physical activity, running, swimming, skiing, soccer, walking, food (excluding “Food and Drug Administration”), eating, nutrition, nutrient, diet, vitamin, calcium, carbohydrates, gluten, caffeine, cholesterol, obesity, and weight. The search retrieved 143 articles. A closer examination revealed that four articles were irrelevant, and these articles were removed. Of the remaining 139 articles, the 80 that were most similar in length were chosen.

SI Scanning Parameters

We captured neural activity during two runs of the article task (500 volumes in each run in study 1 and 311 volumes in each run in study 2) using a T2*-weighted image sequence [repetition time (TR) = 1.5 s, echo time (TE) = 25 ms, flip angle = 70°, -30° tilt relative to the anterior commissure–posterior commissure (AC–PC) line, 54 slices at the Magnetom Tim Trio scanner, 52 slices at the Prisma scanner, field of view (FOV) = 200 mm, slice thickness = 3 mm, multiband acceleration factor = 2, voxel size = 3 × 3 × 3 mm]. High-resolution T1-weighted anatomical images were collected using a magnetization-prepared rapid gradient-echo (MPRAGE) sequence [inversion time (TI) = 1,110 ms, 160 axial slices, voxel size = 0.9 × 0.9 × 1 mm]. Finally, we collected an in-plane, structural, T2-weighted image (slice thickness = 1 mm, 176 axial slices, voxel size = 1 × 1 × 1 mm) to implement a two-stage coregistration procedure between functional and anatomical images.

SI Robustness Checks

To test the robustness of our main results reported in Fig. 1, we estimated models using unranked variables. These analyses produced results similar to those presented in the main text and supported identical conclusions (Fig. S2 and Table S3). Further, models excluding the insignificant direct effects of the two exogenous variables on virality shown in Fig. 1 were estimated to obtain model fit statistics. Both models revealed satisfactory model fit for the hypothesized structural model, considering its small degrees of freedom (df) and small sample size (66): $\chi^2(2) = 2.36$, $P = 0.31$, comparative fit index (CFI) = 0.997, residual mean square error of approximation (RMSEA) = 0.05, 90% CI (0.00, 0.23) for study 1; $\chi^2(2) = 3.26$, $P = 0.20$, CFI = 0.986, RMSEA = 0.09, 90% CI (0.00, 0.26) for study 2. Additional analyses revealed the model fit for the hypothesized path structure was superior to that of alternative structural models (Table S4), providing additional confidence to our proposal that valuation, taking inputs from self and social considerations, serves as a final common pathway.

SI Study 1 Whole-Brain Analysis

To test the specificity of our results to our theory-driven ROIs, we conducted exploratory whole-brain analyses. We first created first-level models for each participant that included a separate boxcar function for activity across all trials within a certain condition (content, reading, broadcasting, narrowcasting) for the reading screen and the rating screen of the article task, respectively (eight regressors). An additional regressor represented the boxcar function representing the reading screen during reading trials modified by a mean-centered parametric modulator of population-level virality ranks of each article. Population-level

virality ranks were derived by ranking all articles presented within the reading condition by their population-level retransmission counts for each participant (range, 1–20). The model also included a boxcar function for activity across all trials within the cue screen and six nuisance regressors to control for motion. Finally, to ensure that only first exposures were modeled in the main regressor of interest, one regressor of no interest was entered to account for trials in which one participant was accidentally presented with an article for a second time. Second, at the group level, neural activity was pooled for all participants to examine the main contrasts of interest: activity during the reading screen in reading trials modulated by population-level retransmission ranks compared with implicit baseline.

To balance the risks of false positives and false negatives, we conducted two different kinds of correction for multiple comparisons to derive whole-brain maps and tables of voxels in which neural activity scales with population-level virality (Fig. S3 and Table S5). The first whole-brain map was thresholded at $P < 0.005$ and $K \geq 320$, where K is the number of voxels per cluster, to produce a threshold of $P < 0.05$, corrected using 3dClustSim simulation (version AFNI 16.2.02). Although the type 2 error rate can be expected to be lower for this method of analysis, prior work has shown that cluster correction tends to overestimate the number of significant voxels and thus increases the type 1 error rate (67). Consequently, we also present the results of a more stringent whole-brain correction that controls the number of false positives more efficiently. Specifically, we used nonparametric permutation testing (5,000 iterations) and false-discovery rate (FDR) correction for a voxelwise P -threshold of $P < 0.05$ and $K \geq 10$ as implemented in the SnPM13 toolbox (68). (Study 1 results for multiple comparisons correction using nonparametric permutation testing corrected at FDR $P < 0.05$ vary across individual runs of the 5,000 permutations protocol implemented here, because of random elements in this analysis technique. Specifically, although several runs produced maps similar to the map printed in Fig. S3, these results border on $P < 0.05$. All runs of the permutation protocol for study 1 produced maps that looked very similar to the one printed here at $P < 0.06$ or $P < 0.07$. Study 2 results are highly robust across several runs of the permutation protocol, $P < 0.05$, FDR corrected.)

SI Study 2 Whole-Brain Analysis

To conduct a parallel whole-brain analysis for study 2 participants, we first created first-level models for each participant that included a separate boxcar function for activity across all trials within a certain condition (abstract, narrowcasting, broadcasting) for the reading screen (three regressors) of the article task. Separate regressors for rating screens were further derived depending on the condition presented on the reading screen (six regressors in total). Crucially, an additional regressor specified the boxcar function representing the reading screen during abstract trials modified by a mean-centered parametric modulator of population-level virality ranks of each article. As for study 1, virality ranks were derived by ranking articles shown within the abstract condition by their population-level retransmission counts for each participant (range, 1–14). The model also included six nuisance regressors to control for motion. Second, at the group level, neural activity during the main task was pooled for all participants to examine the main contrasts of interest: activity during the reading screen in abstract trials modulated by population-level virality ranks compared with the baseline resting state. See *SI Text*, Fig. S3, and Table S4 for details and results.

In parallel to study 1 analyses, whole-brain maps were thresholded via 3dClustSim simulation at $P < 0.005$ and $K \geq 296$ (version AFNI_16.2.02) and nonparametric permutation testing (5,000 iterations) and FDR correction for a voxelwise P -threshold of $P < 0.05$ and $K \geq 10$ as implemented in the SnPM13 toolbox (68). Results are reported in Fig. S3 and Table S5.

SI Analysis of Other Article Task Conditions

In the main text, we focus on neural activity extracted from reading trials in the study 1 article task (Fig. 1) because the reading condition most closely represents real-world experiences of NYTimes readers who are unlikely to visit the website to find an article to share with somebody. Instead, readers are more likely to browse abstracts and consider reading various articles until one article motivates them to share it with somebody else.

Nonetheless, an additional question to consider is the extent to which task instructions affect the relationship between neural activity during article exposure and population-level sharing. Therefore we examined the relationship between value-related neural activity in our value ROI in response to an article's headline and abstract and population-level article retransmission data, focusing separately on narrowcasting trials in which participants were primed before each trial via a cue screen to consider sharing articles with one Facebook friend and broadcasting trials in which participants were primed to consider sharing the article on their Facebook wall. Note that this analysis is not possible for study 2 data, because the other two conditions, not analyzed in the main text, are not comparable to those in study 1 and did not include the presentation of original article abstracts.

Results show that value-related neural activity in response to articles shown in a sharing condition is marginally related to population-level virality in the case of narrowcasting trials [$r = 0.184$, $P = 0.10$] and is not significantly related to population-level virality in the case of broadcasting trials [$r = 0.133$, $P = 0.24$]. Individual-level data from study 1 suggest that explicit instructions to share (i.e., the two sharing conditions) increase the overall level of sharing-relevant brain activity compared with instructions to consider reading the full text of an article (i.e., the reading condition analyzed here; ref. 23). However, we also found that these explicit instructions reduce the variance in value-related activity, which is larger for reading trials ($s^2 = 5.10$) than for narrowcasting ($s^2 = 4.18$) and broadcasting ($s^2 = 3.24$) trials. This ordering of conditions according to variance in information-sharing value corresponds to the condition ordering in terms of the strength of the relationship between value-related activity and population-level virality. If this interpretation is correct, one potential implication could be that sharers are likely to share articles based on "gut" decisions, which are better represented by the reading trials, which did not specifically give participants the goal of sharing in each trial, than by longer elaboration, which is better represented by sharing trials.

SI Article Characteristics

In a content-focused investigation of 760 NYTimes health news articles that included the 80 articles used here, Kim (11) characterized the article headlines and abstracts by analyzing human (i.e., the presence of efficacy information or the mention of diseases or bad health conditions) and computerized (expressed positivity: the difference between the number of positive and negative words; expressed evocativeness/arousal: the sum of positive and negative words) content and with the help of lay human raters (perceived usefulness, induced positivity, perceived controversiality, induced evocativeness/arousal, and perceived novelty). Here we explore the relationship between these content characteristics and concepts within our value-based virality framework as well as population-level virality.

SI Analysis of Article Characteristics

Prior work has shown that content characteristics can impact virality (2, 5), and this argument has been made particularly effectively in the case of news articles (11, 38). Consequently, we explored the role of content characteristics in value-based virality. Specifically, content characteristics might be involved in three different ways. (i) Article characteristics might affect virality directly and independently of variables included in the value-based virality model. If so, it would be of interest whether neural data explain the variance in population-level sharing over and above that explained by article characteristics. (ii) Article characteristics might affect information-sharing value directly or via some other mechanism not currently included in the value-based virality model. (iii) Article characteristics might be antecedents of thoughts regarding the self-related and social outcomes of sharing.

To explore these possibilities, we first checked whether the predictions made by value-based virality (Fig. 1) hold even when controlling for article characteristics. For this purpose, we estimated models identical to the one in Fig. 1 but for the sake of parsimony excluded the insignificant direct effects of self-related and social processing on virality. Each model additionally included a direct effect of one article characteristic on population-level virality. Paralleling other analyses presented in this article, all variables were rank-ordered. In both studies, the effects presented in Fig. 1 were robust when controlling for any of the nine article characteristics considered here. In fact, the only article characteristic that showed a significant effect on population-level virality in these models was the perceived usefulness of an article [B (unstandardized estimate of this parameter) = 0.202, SE = 0.101, $P = 0.04$] in study 1, but this effect did not replicate in study 2.

Second, we examined the relationships between each of the nine content characteristics available to us and average neural activity in regions associated with self-related and social processing in response to each article using t tests and Pearson correlation where appropriate. Paralleling other analyses presented in this article, all variables were rank-ordered.

In study 1, we found a positive relationship between induced positivity in an article and neural activity in the self-related processing ROI [$r = 0.231$; $P = 0.04$]. In addition, articles that mentioned diseases or negative health issues (mean, 9.74) were associated with less self-related processing than articles that did not [mean, 10.70; $T(78) = 2.24$; $P = 0.03$] in study 1. However, these effects did not replicate in study 2.

Finally, we explored direct effects of article characteristics on information-sharing value (i.e., average neural activity in our value-related processing ROI) using analytical strategies identical to those explained above. Value-related neural activity was positively related to the extent to which articles induced positivity in human raters [$r = 0.309$; $P = 0.005$], and articles that mentioned diseases or bad health conditions (mean, 9.50) engaged less value-related activity than articles that did not [mean, 10.96; $T(78) = 3.04$; $P = 0.003$]. However, these effects did not replicate in study 2.

In sum, our results hold, even when controlling for the effects of various article characteristics on virality, suggesting that neural activity contributes information over and above what can be learned from variables commonly used in the literature on virality (11, 38). In contrast to prior work, most article characteristics did not predict population-level sharing. This dissonance with existing studies might be the result of methodological differences among studies. Most notably, previous reports of effects between article characteristics and population-level sharing showed relatively small effect sizes that were identified only in very large samples (e.g., $n > 6,000$ in ref. 38 and $n = 760$ in ref. 11). Because of time restrictions in the fMRI scan, we were not able to replicate these article sample sizes. Nonetheless, our ability to predict

virality from neural variables even in this small sample of articles speaks to the strength and utility of fMRI.

In addition, we identified selected relationships between individual article characteristics and the extent to which articles engaged neural activity associated with self-related, social, or value-related cognition in study 1. Although these relationships generally did not replicate in study 2, these findings might suggest that content characteristics could be promising candidates in the search for antecedents of the psychological processes that affect

sharing. The lack of robustness of these effects might be due to the small sample size and homogeneity of articles. In addition, it is possible that sharing-relevant cognitions are more sensitive to combinations of article characteristics (e.g., the emotional tone in combination with the topic) than to isolated characteristics. However, the specific combination of article characteristics that enhances expectations of positive social or self-related outcomes of sharing might be highly context dependent. An exploration of the large number of potential interaction terms is beyond the scope of this investigation.

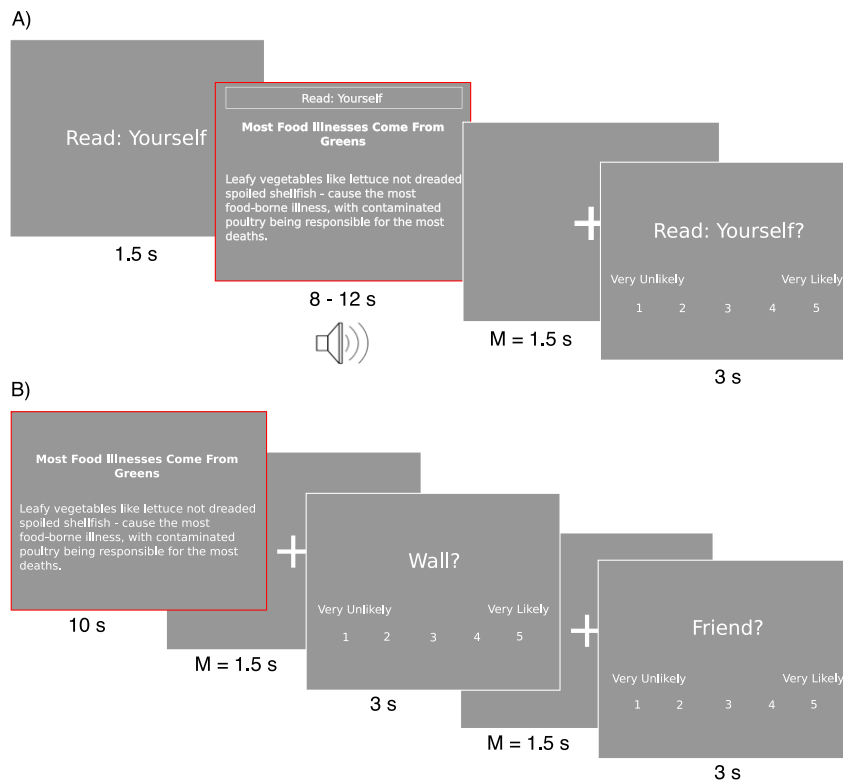


Fig. S1. fMRI tasks. (A) Reading trial of the article task (study 1). (B) Abstract trial of the article task (study 2). The trial modeled in main analyses is marked in red.

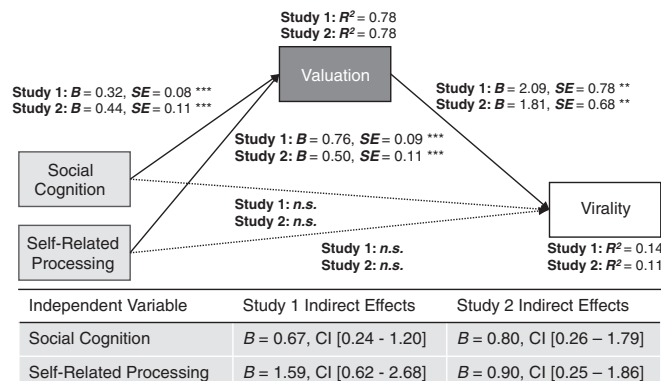


Fig. S2. Value-based virality path model including unranked variables. The path diagram shows maximum likelihood estimates (unstandardized coefficients). The table presents indirect effect coefficients and bias-corrected, bootstrapped 95% CIs (1,000 replications). Population-level virality was log-transformed because of its positively skewed distribution. $n = 80$ in study 1 and 76 in study 2; * $P < 0.05$, ** $P < 0.01$, *** $P < 0.001$, n.s., not significant.

Table S1. ROIs in study 1 and study 2

ROI	Volume, cm ³	Center of mass		
		x	y	z
Self-related processing				
Ventromedial prefrontal cortex	0.23	-4.26	56.6	-3.92
Precuneus/posterior cingulate cortex	1.93	-6.68	-55	28.2
Valuation				
Ventral striatum	4	-3	10	-4
Ventromedial prefrontal cortex	3.59	1	46	-7
Social processing				
Middle-medial prefrontal cortex	2.4	1.91	55	11.6
Dorsomedial prefrontal cortex	2.61	-0.13	53.7	29.3
Right temporoparietal junction	3.0	54.1	-52.6	23.1
Left temporoparietal junction	3.0	-51.7	-58.3	24.8
Right superior temporal lobe	3.1	54.4	-8.45	-17.3

The x, y, and z coordinates correspond to the MNI standard brain. All neural systems and subclusters are defined based on prior studies as described in *Methods*.

Table S2. Correlation matrices underlying the path models in Fig. 1 (variables 1–4) and Fig. S4 (variables 1–5)

Variable	1	2	3	4	5
Study 1, n = 80					
1. Self-related processing ROI	1				
2. Social processing ROI	0.705***	1			
3. Valuation ROI	0.838***	0.702***	1		
4. Population-level virality	0.240*	0.253*	0.387***	1	
5. Self-reported intentions	0.125	0.263*	0.285*	0.337**	1
Study 2, n = 76					
1. Self-related processing ROI	1				
2. Social processing ROI	0.822***	1			
3. Valuation ROI	0.814***	0.770***	1		
4. Population-level virality	0.094	0.182	0.237*	1	
5. Self-reported intentions	0.146	0.164	0.191	0.372***	1

Asterisks indicate statistical significance: * $P < 0.05$, ** $P < 0.01$, *** $P < 0.001$.

Table S3. Correlation matrices underlying the path model in Fig. S2 that includes unranked variables

Variable	1	2	3	4
Study 1, n = 80				
1. Self-related processing ROI	1			
2. Social processing ROI	0.717***	1		
3. Valuation ROI	0.856***	0.758***	1	
4. Population-level virality	0.236*	0.235*	0.352**	1
Study 2, n = 76				
1. Self-related processing ROI	1			
2. Social processing ROI	0.868***	1		
3. Valuation ROI	0.859***	0.851***	1	
4. Population-level virality	0.107	0.163	0.256*	1

Population-level virality showed a positively skewed distribution and thus was log-transformed. Asterisks indicate statistical significance: * $P < 0.05$, ** $P < 0.01$, *** $P < 0.001$.

Table S4. Model fit comparison for alternative path structures

Model	χ^2 (df), <i>P</i>	CFI	RMSEA (90% CI)	AIC	BIC
Study 1, <i>n</i> = 80					
(A) Valuation mediates	2.36 (2), 0.31	0.997	0.05 (0.00–0.23)	1,593.80	1,605.71
(B) Self-related processing mediates	10.63 (2), 0.01	0.925	0.23 (0.11–0.38)	1,602.08	1,613.99
(C) Social cognition mediates	10.08 (2), 0.01	0.888	0.23 (0.10–0.37)	1,601.53	1,613.44
Study 2, <i>n</i> = 76					
(A) Valuation mediates	3.26 (2), 0.20	0.986	0.09 (0.00–0.26)	1,457.07	1,468.72
(B) Self-related processing mediates	6.98 (2), 0.03	0.955	0.18 (0.05–0.34)	1,460.79	1,472.44
(C) Social cognition mediates	5.09 (2), 0.08	0.968	0.14 (0.00–0.30)	1,458.90	1,470.56

(A) represents a model resembling the path model in Fig.1 excluding the two insignificant effects. (B) represents a version of model A in which the roles of "valuation" and "self-related processing" are switched. (C) represents a version of model A in which the roles of "valuation" and "social cognition" are switched. AIC, Akaike's information criterion; BIC, Bayesian information criterion.

Table S5. Whole-brain tables: Clusters significantly associated with population-level virality ranks of the NYTimes articles shown in each trial during reading screen periods (study 1) or abstract trials (study 2)

Region	R/L	x	y	z	Cluster		Nonparametric	
					T	K	T	K
Study 1								
Medial prefrontal cortex*	L	−3	59	1	4.52	1495	4.52	90
Anterior cingulate cortex	L	−3	47	10	4.27		4.28	
Caudate [†]	R	3	8	−5	2.97			
Dorsomedial prefrontal cortex	L	−12	38	31	4.08		4.09	14
Dorsomedial prefrontal cortex [†]	R	6	65	25	3.22			
Dorsolateral prefrontal cortex/superior frontal gyrus	L	−27	53	31	3.28		3.28	11
Ventromedial prefrontal cortex	L	−3	38	−11	4.23		4.24	11
Lateral orbital frontal cortex	L	−21	62	10	4.08		4.09	48
Mid cingulate cortex*	L	−6	−16	34	4.56	549	4.57	129
Mid cingulate cortex	M	0	−22	40	4.33		4.33	
Precuneus [†]	L	−18	−49	31	4.09			
Cingulate [†]	R	12	−28	28	3.84			
Thalamus	L	−4	−28	7	—		3.05	32
Study 2								
Medial prefrontal cortex	R	15	50	1	4.76	2,698	4.77	905
Medial prefrontal cortex	L	−15	50	−2	4.42		4.43	
Ventromedial prefrontal cortex	R	3	38	−8	3.67		3.67	
Anterior cingulate cortex*	L	−3	32	10	5.33		5.34	
Caudate	R	3	8	4	4.73		4.74	
Putamen	R	15	8	−8	3.88		3.89	
Caudate	L	−12	20	1	4.59		4.61	
Caudate	R	12	17	1	3.99		4.01	
Posterior cingulate cortex*	R	3	−40	19	4.48	506	4.50	126
Posterior cingulate cortex	R	6	−22	31	3.99		4.00	
Posterior cingulate cortex	L	−9	−43	19	3.70		3.72	

Clusters significantly associated with population-level virality ranks of the NYTimes articles shown in each trial during reading screen periods of reading (study 1) or abstract trials (study 2). The *x*, *y*, and *z* coordinates correspond to the MNI standard brain. No suprathreshold clusters were observed that were negatively associated with the parametric modulator. Thresholding: For each study, voxels significant under cluster correction and voxels significant under nonparametric correction are shown. Cluster correction thresholding was performed based on 3dClustSim simulation at *P* < 0.005 uncorrected and *K* ≥ 320 in study 1 and *K* ≥ 296 in study 2; nonparametric thresholding was performed through nonparametric permutation testing and FDR *P* < 0.05, *K* > 10. Separate clusters in the cluster-corrected map are divided by spaces between rows. *df* = 1, 38; voxel size = 3 × 3 × 3 mm. *K*, number of voxels per cluster. L, left; M, medial; R, right.

*Peak voxel within cluster.

[†]Peaks that are present only under cluster correction.